Environmental Science & Technology

pubs.acs.org/est

Article

Unveiling the Role of Sulfur in Rapid Defluorination of Florfenicol by Sulfidized Nanoscale Zero-Valent Iron in Water under Ambient Conditions

Zhen Cao, Hao Li, Gregory V. Lowry, Xiaoyang Shi, Xiangcheng Pan, Xinhua Xu, Graeme Henkelman, and Jiang Xu*

Cite This: *Environ. Sci. Technol.* 2021, 55, 2628−2638

Read Online

ACCESS | Metrics & More | Article Recommendations | Supporting Information

ABSTRACT: Groundwater contamination by halogenated organic compounds, especially fluorinated ones, threatens freshwater sources globally. Sulfidized nanoscale zero-valent iron (SNZVI), which is demonstrably effective for dechlorination of groundwater contaminants, has not been well explored for defluorination. Here, we show that SNZVI nanoparticles synthesized via a modified post-sulfidation method provide rapid dechlorination (∼1100 μmol m^{-2} day^{-1}) and relatively fast defluorination (∼6 μmol m^{-2} day^{-1}) of a halogenated emerging contaminant (florfenicol) under ambient conditions, the fastest rates that have ever been reported for Fe^0-based technologies. Batch reactivity experiments, material characterizations, and theoretical calculations indicate that coating S onto the metallic Fe surface provides a highly chemically reactive surface and changes the primary dechlorination pathway from atomic H for nanoscale zero-valent iron (NZVI) to electron transfer for SNZVI. S and Fe sites are responsible for the direct electron transfer and atomic H-mediated reaction, respectively, and β-elimination is the primary defluorination pathway. Notably, the Cl atoms in florfenicol make the surface more chemically reactive for defluorination, either by increasing florfenicol adsorption or by electronic effects. The defluorination rate by SNZVI is ∼132−222 times higher with chlorine attached compared to the absence of chlorine in the molecule. These mechanistic insights could lead to new SNZVI materials for in situ groundwater remediation of fluorinated contaminants.

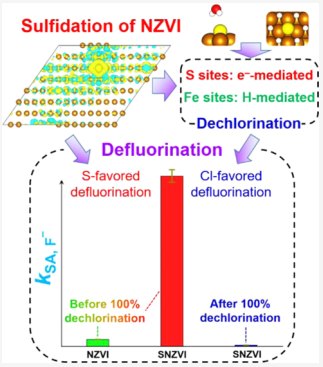

KEYWORDS: *Defluorination, Reactive site, Environmental nanotechnology, Environmental remediation, Sulfidized nanoscale zerovalent iron*

1. INTRODUCTION

Defluorination of fluorinated organic contaminants is challenging in environmental remediation due to the high stability of the C−F bond at the ambient conditions for the reactions. Activation of C−F bonds usually requires an organometallic catalyst, e.g., transition metals (especially noble catalysts like Pd and Rh) and high temperatures,[1−4] which are not practicable for in situ groundwater remediation. Although a promising groundwater remediation agent for dechlorination,[5−8] nanoscale zero-valent iron (NZVI) is not able to readily defluorinate contaminants under ambient conditions.[9,10]

Recently, sulfidation of NZVI (SNZVI) has been proven to suppress reactions with water and improve the reactivity and selectivity for chlorinated organics.[11−14] A combination of hydrophobicity and enhanced electron transfer is touted as the main benefit of NZVI sulfidation,[15−19] and this was recently confirmed using electrochemical tests and water contact angle measurements.[20] However, these characterizations are both bulk analyses, so it is unclear if the reactive sites are Fe or S sites and how sulfur affects the charge density distribution of SNZVI at an atomistic level. Both NZVI and SNZVI afford the hydrogen evolution reaction (HER) in water,[11−13] which involves the generation of atomic H (Volmer reaction) via electron transfer from the materials to water and its subsequent combination to form H_2 (Tafel or Heyrovsky reaction) on a metal surface.[21,22] Although previous studies have shown that H_2, atomic H, and direct electron transfer are all capable of reducing chlorinated compounds by NZVI or bimetallic NZVI (e.g., Ni−Fe and Pd−Fe),[5,12,23] the role of these reactive species in SNZVI reactivity remains unclear. A better understanding of these reactive sites and species will improve our conceptual model of dechlorination and defluorination by SNZVI.

Defluorination of fluorinated contaminants under ambient conditions is attractive, and the physicochemical properties of SNZVI (e.g., hydrophobicity and electron transfer) make it

Received: October 29, 2020
Revised: January 12, 2021
Accepted: January 20, 2021
Published: February 2, 2021

Downloaded via UNIV OF TEXAS AT AUSTIN on March 30, 2021 at 23:34:17 (UTC).
See https://pubs.acs.org/sharingguidelines for options on how to legitimately share published articles.

ACS Publications © 2021 American Chemical Society

https://dx.doi.org/10.1021/acs.est.0c07319
Environ. Sci. Technol. 2021, 55, 2628−2638

possible for the SNZVI to selectively react with the contaminant but not water, unlike other advanced oxidation or reduction technologies that split much more water than reacting with the contaminant. SNZVI materials are synthesized mainly through co-sulfidation methods (i.e., reduction of Fe ions in the presence of a reduced S reagent)[24,25] or conventional post-sulfidation methods (i.e., adding a reduced S reagent like Na_2S into an NZVI suspension).[26] Although ∼30% of florfenicol (FF) was defluorinated by SNZVI (synthesized by an Fe^{2+} precursor) after 4 months in our previous study,[17] this defluorination rate was relatively too slow to apply the SNZVI for an in situ groundwater remediation scenario, e.g., permeable reactive barrier. Our recent study has proved that the reactivity of both NZVI and SNZVI could be greatly improved if using an Fe^{3+} precursor rather than an Fe^{2+} precursor,[27] and the defluorination capability of SNZVI synthesized by an Fe^{3+} precursor via common sulfidation methods was greatly improved.[28] However, both the sulfidation efficiency ($[S/Fe]_{particle}/[S/Fe]_{dose}$) (0.9−13.6%) and the specific surface area (10−42 m^{-2} g^{-1}) of SNZVI synthesized by conventional post-sulfidation methods were relatively low,[28] despite changing the sulfur precursors and their addition procedure. It is unclear if increasing the actual S content and surface area could further improve the defluorination capability of SNZVI. Moreover, the reactive sites and species for defluorination remain unclear, the defluorination pathway was not confirmed, and the impacts of molecular structure and adsorption of the contaminant on the charge density distribution of SNZVI were unknown, preventing the rational design of SNZVI materials and application scenarios. A better understanding of why SNZVI is reactive with C−F bonds under ambient conditions will promote the use of SNZVI and its derivatives for defluorination of emerging groundwater contaminants.

Herein, SNZVI nanoparticles that provide rapid dechlorination and defluorination of FF, but suppressed HER, were synthesized using an Fe^{3+} precursor to synthesize NZVI (Figure S1), followed by addition of Fe^{2+} and then Na_2S to provide particles with a high sulfur content and surface area. FF, a frequently detected antibiotic and emerging environmental contaminant,[29,30] was selected as the reactivity probe. Traditional water treatment methods could not efficiently degrade FF, and residual FF in water could lead to antibiotic resistance. Moreover, FF has Cl and F groups on the same molecule, which allows for a direct comparison of the reactivities of Cl versus F leaving groups. Multiple approaches, including experimental data correlations, quenching experiments, various characterizations, ultraperformance liquid chromatography-tandem mass spectrometer (UPLC-MS/MS), and density functional theory (DFT) calculations, were used to identify the reactive sites and the species responsible for dechlorination and defluorination at both bulk and atomistic levels.

2. EXPERIMENTAL SECTION

2.1. Materials. $FeCl_3$ (≥97%), $NaBH_4$ (≥98%), $FeSO_4 \cdot 7H_2O$ (99−101%), $Na_2S \cdot 9H_2O$ (≥98%), NaF (≥98%), HCl (37%), NaOH (≥96%), and HNO_3 (65−68%) were obtained from Sinopharm Group Chemical Reagent Co., Ltd. Florfenicol (FF, >99%), and the standards of their dechlorinated products (deschloro FF and dideschloro FF) were obtained from Shanghai Ruichu Biotech Co., Ltd. and Absin Bioscience Inc., respectively. *tert*-Butanol (TBA, ≥99.5%) was obtained from Aladdin Reagent Co., Ltd. Deionized water after nitrogen purging for 1 h was used in all cases.

2.2. Preparation of NZVI and SNZVI. NZVI particles were synthesized by a widely reported borohydride method.[31] Briefly, 100 mL of 5.10 g L^{-1} $NaBH_4$ solution was dropwise added (∼10 mL min^{-1}) into a 500 mL three-necked flask containing 175 mL of 1.43 g L^{-1} Fe^{3+} solution under stirring (500 rpm) and nitrogen purging. SNZVI particles were synthesized with a modification of the commonly reported post-sulfidation method.[26,32−34] A certain amount of extra Fe^{2+} (0.018, 0.035, 0.053, or 0.070 g, respectively) was dissolved in 100 mL of 2.50 g L^{-1} as-prepared NZVI suspension by continuously stirring for 10 min, and then 50 mL of Na_2S solution (0.24, 0.48, 0.72, or 0.96 g L^{-1}, respectively) was added dropwise (∼5 mL min^{-1}) into the mixture of NZVI−Fe^{2+} under stirring and nitrogen purging. The theoretical value of the S/Fe molar ratio ($[S/Fe]_{dose}$) was 0.07, 0.12, 0.17, and 0.22, respectively. The as-prepared NZVI and SNZVI particles were washed three times by deionized water and ethanol, and then vacuum-dried before use.

2.3. Batch Experiments. Batch reactivity experiments of NZVI or SNZVI with water were conducted in 60 mL glass vials containing 20 mL of 1 g L^{-1} NZVI or SNZVI suspension and 40 mL headspace, which were capped by Teflon Mininert valves and located on a temperature-controlled horizontal shaker (100 rpm) at 25 °C. The H_2 in the headspace was monitored over 15 days to assess the ability of each material for HER. The degradation of FF by NZVI or SNZVI over 15 days was conducted in the same type of sealed 500 mL glass vials containing 250 mL of 0.28 mM FF solution and 1 g L^{-1} of each material, shaking at the same speed and temperature. Aqueous samples were collected and filtered by a 0.45 μm poly(ether sulfone) membrane before analysis. Unless specified, basic experimental conditions were as follows: initial pH = 7.0, T = 25 °C, 0.28 mM FF, and 1.0 g L^{-1} NZVI or SNZVI.

Different concentrations (1−1000 mM) of TBA, a scavenger for both atomic H ($(1.0-11.5) \times 10^5$ M^{-1} s^{-1})[35−37] and hydroxyl radicals ($^{\bullet}OH$),[38] were added to study the role of atomic H in the FF degradation by SNZVI ($[S/Fe]_{dose}$ = 0.07). Since the increase of TBA from 1 to 500 mM did not further inhibit the dechlorination of SNZVI as discussed later, the concentrations of FF and Cl^- for 1000 mM TBA with SNZVI were not monitored, while the F^- concentrations of the initial stage (2 h) and long-term reaction (15 days) were measured to assess their impact on the defluorination.

2.4. Analytical Methods. The Fe^0 content was calculated by measuring the generated H_2 after the acidification of ∼20 mg of each material by 10 mL of HCl.[5,39] The actual S/Fe molar ratio in SNZVI particles ($[S/Fe]_{particles}$) was determined by inductively coupled plasma-optical emission spectroscopy (ICP-OES, Optima 8300DV) after the digestion of ∼10 mg SNZVI in 15 mL of aqua regia for 5 h.[40,41]

FF and dechlorinated products were quantified by high-performance liquid chromatography (HPLC, Shimadzu, Japan), and the defluorinated products were analyzed by UPLC-MS/MS (Waters Xevo TQ-S) in negative ion mode $[M - H]^-$ (ESI^-) as previously described.[17,42]

H_2 was analyzed by a gas chromatography-thermal conductivity detector (GC-TCD) system (Agilent 7890A) equipped with a Molsieve 5 Å/Poranod Q column and a carrier gas (argon). The injection volume was 500 μL, and the temperatures of the oven, sample injector, and detector were

https://dx.doi.org/10.1021/acs.est.0c07319
Environ. Sci. Technol. 2021, 55, 2628−2638

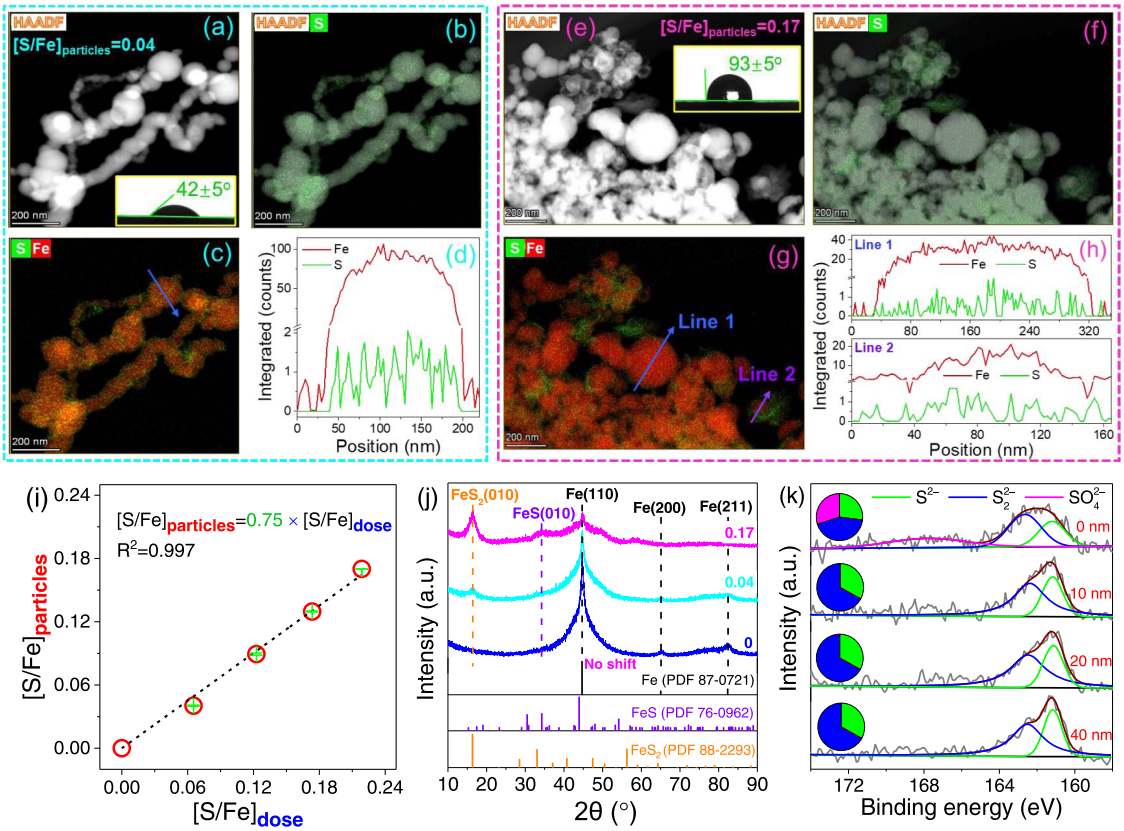

Figure 1. Morphology and Fe and S distributions of SNZVI with (a−d) $[S/Fe]_{particles}$ = 0.04 and (e−h) $[S/Fe]_{particles}$ = 0.17 determined by TEM-energy-dispersive X-ray (EDX)-mapping analysis. Insets show the water contact angles of SNZVI pellets. (i) Positively linear correlation of actual $[S/Fe]_{particles}$ with $[S/Fe]_{dose}$. (j) XRD spectra of NZVI and SNZVI. (k) XPS depth profiles of sulfur speciation for SNZVI with $[S/Fe]_{particles}$ = 0.04.

45, 110, and 250 °C, respectively. At the end of a single detection procedure, the oven temperature was increased to 150 °C for 5 min to clear the residual organic matter and water.

Aqueous F^-, Cl^-, and SO_4^{2-} were determined by an ion chromatograph (IC, Metrohm 883 basic IC) equipped with a Metrosep A Supp 5 column (150 mm L × 4.0 mm ID). The eluent was 3.2 mM Na_2CO_3 and 1.0 mM $NaHCO_3$ at a flow rate of 0.7 mL min^{-1}; the sample volume was 20 μL. The retention times of F^-, Cl^-, and SO_4^{2-} were 3.3, 5.1, and 14.0 min, respectively. Note that the release of sulfur from the particles (<0.08% of the actual S content) was limited (SO_4^{2-} < 0.03 mg L^{-1}), consistent with a previous study.[43] Moreover, the F^- in the solution after 15 days of reaction was double-checked by a portable multimeter (HACH HQ40d) with a fluoride ion-selective electrode, which was close to the results of IC (the discrepancy was about 5%). The detection limits of IC and the fluoride ion-selective electrode for F^- were 0.05 and 0.02 ppm, respectively.

Various techniques were used to characterize the materials as previously reported.[25,44−47] Transmission electron microscopy (TEM, FEI Tecnai G2 F20) and Brunauer−Emmett−Teller (BET) analysis (MicroActive ASAP 2460) were applied to characterize the morphology and surface area, respectively.[48,49] The depth profile of X-ray photoelectron spectroscopy (XPS, Thermo Scientific K-Alpha) was used to characterize the speciation and distribution of iron and sulfur over the particles as previously reported.[13,41,44] X-ray diffraction (XRD, Bruker D8 Advance) was used to characterize the crystalline structures of NZVI and SNZVI. Water contact angles of pellets made from NZVI and SNZVI materials were measured to describe the hydrophobicity of materials.[13] Electrochemical characterizations, including the open-circuit potential (OCP) analysis, electrochemical impedance spectroscopy (EIS), and linear sweep voltammetry (LSV), were performed with a potentiostat (VMP3, Bio-Logic Science Instruments) to describe the corrosion tendency, charge-transfer resistance, and HER of materials, respectively, as previously described.[41] Note that the contact resistance of the electrodes was assumed to be the same as all of the samples were prepared by the same pressure (5 tons) and material weight (∼40 mg), and the observed differences of R_2 reflect differences in the electron-transfer resistance of the materials.

2.5. Computational Method. Density functional theory (DFT) calculations with spin polarization were performed using the VASP package to understand the role of S in the hydrophobicity, blocking H adsorption at Fe sites, and charge density in the system, as well as the most favorable configuration of the FF molecule on Fe surfaces. The adsorption geometries of water and H at the Fe(110) surface were evaluated with various numbers of S atoms on the surface. The selection of S atoms on the surface of the Fe(110) model, rather than S atoms combined into the Fe(110) crystalline structure, was based on the XRD analysis, which shows that sulfur did not change the crystalline structure (Figure 1j).

The core electrons were described by the projector augmented-wave method.[50] The electronic exchange and correlation were estimated by the generalized gradient approximation method with the functional developed by Perdew, Burke, and Ernzerhof.[51] Kohn−Sham wave functions

https://dx.doi.org/10.1021/acs.est.0c07319
Environ. Sci. Technol. 2021, 55, 2628−2638

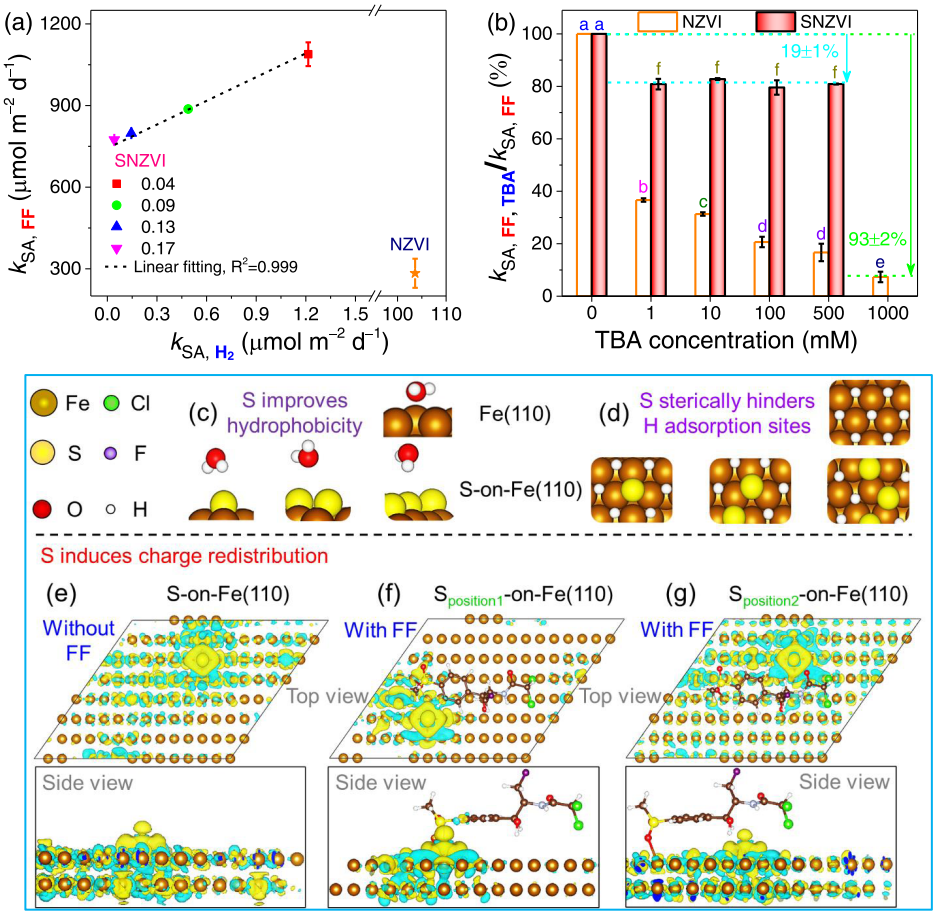

Figure 2. (a) Correlation of FF dechlorination rate ($k_{SA,FF}$) with HER ability (k_{SA,H_2}). (b) Impact of atomic H scavenger (TBA) on the $k_{SA,FF}$ by NZVI and SNZVI with 0.04 $[S/Fe]_{particles}$. $k_{SA,FF,TBA}$ represents the surface-area-normalized rate of FF dechlorination by NZVI and SNZVI in the presence of TBA. Different letters indicate significantly different values ($\alpha = 0.05$; one-way analysis of variance (ANOVA)). Basic conditions: initial pH = 7.0, T = 25 °C, 0.28 mM FF, and 1.0 g L^{-1} NZVI or SNZVI. Impact of S on (c) H_2O and (d) H adsorption geometries. (e−g) DFT-calculated S-induced charge density redistribution on Fe(110) surfaces (yellow and cyan colors represent higher and lower electron charge densities, respectively).

were expanded on a plane wave basis to describe the valance electrons.[52] The Brillouin zone was sampled with a (3 × 3 × 1) k-point mesh using the method of Monkhorst and Pack.[53] The kinetic energy cutoff was set as 400 eV. The force convergence criterion was set as 0.05 eV $Å^{-1}$. We did not analyze the adsorption of Cl in our DFT calculations. For the calculations of H_2O and H adsorption, a four-layer (3 × 3) Fe(110) slab was modeled. For the calculation of the adsorption of FF and FF-related species, a two-layer (14 × 14) Fe(110) slab was modeled, due to the large size of the FF molecule. A vacuum layer of at least 12 Å was used to separate periodic images. Note that we used a general model to analyze the effect of S on the hydrophobicity and H-blocking capacity on an Fe surface, by tuning the number of S atoms from 1 to 3 (Figure 2c,d), which was close to 0.03−0.08 S/Fe ratios in the SNZVI used here. Since our experiments consist of multiple Fe−S phases that are difficult to disentangle, we cannot propose specific and compositionally dependent models for a more quantitative understanding in DFT. However, using combined extended X-ray-absorption fine structure (EXAFS) and DFT,[20] one of our most recent studies showed that a general model by doping S to Fe surfaces can help understand the role of sulfur in the hydrophobicity, H-blocking capacity, and reactivity in SNZVI. As for the adsorption of FF and the FF derivatives, we did not focus on the compositional effect of the S/Fe ratios, due to the significant cost of computation in this study (with a (14 × 14) reactive surface and the large number of possible molecular configurations using spin-polarized DFT). The calculated absolute binding energy of S on an Fe surface was −5.91 eV, indicating that a S atom can be strongly stabilized on an Fe surface. To find the most favorable configuration, multiple adsorption configurations of FF on the Fe(110) surface were considered, and the most energetically favorable configuration was selected for further evaluation. The adsorption energies (E_{ads}) of FF and FF-related species on Fe(110) were calculated by

$$E_{ads} = E_{ads^*} - E_{bare} - E_{mol}$$

where E_{ads^*} is the total energy of the surface with the adsorbed molecule, E_{bare} is the total energy of a bare surface, and E_{mol} is the total energy of the adsorbate molecule in a vacuum.

3. RESULTS AND DISCUSSION

3.1. Characterizations. Conventional post-sulfidation is only able to coat a limited amount of sulfur onto NZVI particles and does not change its chainlike structure (Figure S2).[54] In contrast, more sulfur was coated onto the NZVI surface because of the pre-adsorbed Fe^{2+}; ∼75% of the dosed

https://dx.doi.org/10.1021/acs.est.0c07319
Environ. Sci. Technol. 2021, 55, 2628−2638

sulfur was detected in the particles (Figure 1i), making the particles more hydrophobic (Figure S3a) due to the hydrophobic character of iron sulfides.[55,56] Sulfur was well distributed over the chainlike particles of SNZVI with a low $[S/Fe]_{particles}$ (0.04) according to the S and Fe maps and line scans (Figures 1a−d and S4). For the SNZVI particles with a high $[S/Fe]_{particles}$ (0.17) (Figures 1e−h and S5), the primary particles show a relatively even distribution of S (line 1 in Figure 1h), while flocculent substances enriched with S (line 2 in Figure 1h and line 4 in Figure S5f) and hollow particles (line 3 in Figure S5f) were also observed. These elemental distribution maps and line scans reveal an uneven distribution of S over the $[S/Fe]_{particles}$ = 0.17 particles, which changed its properties and reactivity as discussed below, e.g., particles with the hollow structure would have a lower reactivity for dechlorination.[41] The surface area (88.5−145.4 m^2 g^{-1}) of SNZVI increased with increasing S content (Figure S3c), likely due to increasing surface roughness and the formed flocculent. These values were 7.5−12.3, 14−22, and 3−23 times higher than those of unsulfidized NZVI in this study, previously reported unsulfidized NZVI,[57,58] and previously reported SNZVI,[24,32] respectively.

Iron sulfides (FeS_2 and FeS) were identified in the XRD spectra of SNZVI with a high sulfur amount (Figure 1j), which has rarely been detected by XRD before (i.e., either amorphous or below the detection limit). While S incorporated into the Fe body-centered cubic (BCC) structure could shift the typical peaks of Fe^0 and expand the lattice,[20] neither a shift (Figure 1j) nor an expansion (Figure S6) was observed in this study, suggesting that S was not incorporated into the Fe BCC structure; rather, there was a high possibility that S was present as a surface layer. XRD only detects crystalline phases and reveals the bulk speciation, so XPS analysis using a sputtering depth profile was conducted on the most reactive material ($[S/Fe]_{particle}$ = 0.04 as discussed later). Relatively more oxidized forms of Fe and S species were detected on the surface of the particles (Figures 1k and S7), while no oxidized S species was observed for the inner phase (deeper than 10 nm). The majority of S on the particles was in the reduced forms (S^{2-} and S_2^{2-}), consistent with the XRD spectra (Figure 1j) and previous reports for conventional sulfidation methods.[20,59]

The surface-area-normalized rates of H_2 evolution (k_{SA,H_2}) by SNZVI reaction with water (Figure S8a−c) were 50−1500, 7−657, and 3−80 times lower than that of unsulfidized NZVI, conventional post-sulfidized SNZVI by Na_2S (without Fe^{2+}), and a hydrophobic co-sulfidized SNZVI, respectively.[13,32] Besides the improved hydrophobicity, the decreased corrosion tendency and charge-transfer rate also contributed to the inhibited HER ability according to the electrochemical tests (Figure S9). This significantly suppressed water reactivity of SNZVI could improve the electron selectivity for target contaminants over water and prolong its reactive lifetime (Figure S8d). In addition, the lower corrosion tendency and charge-transfer rate at higher S loading were consistent with the decreased Fe^0 content (Figure S3b) and uneven distribution of S (Figure 1e−h), and resulted in lower reactivity as discussed below.

3.2. Reactive Species for Dechlorination. The suppressed reactivity of SNZVI nanoparticles with water makes them attractive but only if they remain reactive (or are even more reactive) with target contaminants. Batch reactivity experiments show that almost all of the FF was removed within 15 min by SNZVI, with no H_2 detected (Figure S10), regardless of the sulfur amount, suggesting that SNZVI with a robust reactivity and a high electron efficiency (∼100% of the electrons from SNZVI reduce FF rather than water) is a promising material for antibiotic FF removal.

The reactive species (H_2, atomic H, or electrons) for the FF reductive dechlorination by SNZVI were further investigated. The surface-area-normalized dechlorination rate of FF ($k_{SA,FF}$) by SNZVI had a positive correlation to their HER rate (k_{SA,H_2}) (Figure 2a). Since SNZVI could not utilize the H_2 for dechlorination,[12] this correlation suggests that atomic hydrogen atoms and electrons involved in the HER could be possible reactive species for the FF dechlorination. Their fraction in dechlorination was further confirmed by a quenching experiment using an atomic H scavenger, *tert*-butanol (TBA).[35,37,60] The dechlorination became slower in the presence of TBA (Figures 2b and S11b), but increasing the TBA did not further inhibit the dechlorination, suggesting that ∼20% of dechlorination was attributed to atomic H, and the majority of FF was dechlorinated via direct electron transfer. In contrast, more than 93% of FF was removed by NZVI via atomic H (Figures 2b and S11a). These results suggest that sulfidation changed the surface reactivity by altering the reactive species for dechlorination.

3.3. Impact of Sulfur on the Fe Surfaces and Reactive Sites. DFT calculations were performed to further understand the reason why sulfur changes the surface reactivity and the reactive species, as well as how the Fe and S sites behave under reaction conditions. The above characterizations suggest that the material is a kind of mixture, i.e., S-coated NZVI and an FeS-like substance. However, it was reported that the reactivity of S-coated NZVI for dechlorination is much higher than those of bare NZVI (∼14-fold) and FeS (∼50-fold),[41,61] suggesting that the S-coated surface controls the reactivity. Our results also show that further increasing the FeS-like substance did not increase the reactivity (e.g., the $[S/Fe]_{particles}$ = 0.17 material as compared to the $[S/Fe]_{particles}$ = 0.04 material in Figure 1c,g,i). Since sulfur did not incorporate into the Fe BCC structure (Figure 1j), a model consisting of S atoms sitting on the Fe BCC surface is suitable to investigate the reactivity of SNZVI at an atomistic level.

While sulfur incorporated into the Fe BCC structure was proven to be hydrophobic,[20] DFT calculations on the H_2O adsorption geometries show that the sulfur on the Fe(110) surface (S-on-Fe(110)) can also improve the materials' hydrophobicity (Figure 2c), consistent with water contact angle measurements (Figure S3a). Note that similar calculations on FeS and FeS_2 structures (mackinawite and pyrite, respectively) were performed in our recent study,[20] and no significantly different conclusion (i.e., the S site is hydrophobic and the presence of S hinders H adsorption at Fe sites) was found compared to our current model with sulfur-doped Fe (Table S1). This could favor the adsorption of hydrophobic contaminants or contaminants with hydrophobic groups (e.g., Cl and F groups) and inhibit reactions with water, which would increase the selectivity for contaminants' decomposition. However, the S site also physically hinders the adsorption sites of H on the Fe surface (Figure 2d), which is expected to decrease the coverage of adsorbed atomic H and inhibit the H-mediated dechlorination, consistent with the decreased FF dechlorination rate with increasing sulfur content (Figure 2a). Interestingly, a sulfur atom on the Fe(110) surface can cause a

https://dx.doi.org/10.1021/acs.est.0c07319
Environ. Sci. Technol. 2021, 55, 2628−2638

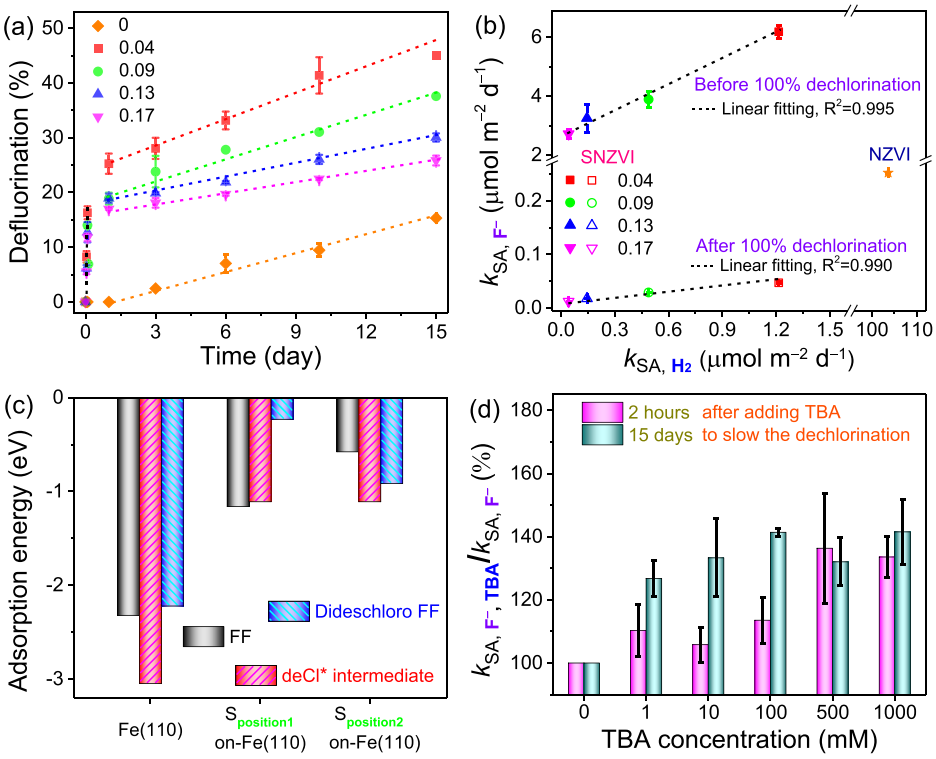

Figure 3. (a) Defluorination efficiencies of FF by NZVI or SNZVI according to aqueous F^- ion measurements. (b) Comparison of the FF defluorination rate (k_{SA,F^-}) before and after its complete dechlorination and its correlation with HER ability (k_{SA,H_2}). Basic conditions: initial pH = 7.0, T = 25 °C, 0.28 mM FF, and 1.0 g L^{-1} NZVI or SNZVI. (c) DFT-calculated adsorption energy of FF, dechlorinated intermediate, and dideschloro FF on the Fe(110) and S-on-Fe(110) surfaces. (d) Improved FF defluorination by SNZVI (0.04 $[S/Fe]_{particles}$) in the presence of TBA. $k_{SA,F^-,TBA}$ represents the surface-area-normalized rate of FF defluorination by SNZVI in the presence of TBA.

significant redistribution of charge density on the Fe sites (Figure 2e), which may increase the density of localized unpaired electrons, making the surface highly chemically reactive, and promoting the subsequent reactions.[62,63] This significant change of surface reactivity is a possible reason for why the NZVI plot deviates significantly from the linear trend of SNZVI in the correlation between dechlorination reactivity and HER activity (Figure 2a).

Moreover, the presence of S attracts electronic charge from nearby Fe sites (Figure 2e). Given that the S site is hydrophobic (Figure 2c) and blocks H adsorption at Fe sites (Figure 2d), this electron redistribution suggests that the S site is reactive for direct electron transfer but limits atomic H-mediated reaction. Meanwhile, according to the famous d-band center theory,[64] the loss of electron charge may lead to a decrease in the d-band filling at these Fe sites, which in turn promotes the adsorption and decomposition capability for contaminants. This is consistent with the experimental results that SNZVI is highly reactive than NZVI (Figure 2a), and the majority of FF was dechlorinated via direct electron transfer (Figure 2b). In contrast, since S sites are very hydrophobic, water dissociation (Volmer step) could only occur at the Fe sites, as is well established for the HER on metal surfaces,[65] suggesting that the reactive Fe sites are responsible for the atomic H-mediated dechlorination.

3.4. Cl Group in an FF Molecule Favors Its Defluorination by SNZVI. Although the defluorination (the half-life of 0.28 mM FF by SNZVI was 17.4−53.2 days for the long-term reaction) is much slower than dechlorination (the half-life was 3.6−4.5 min), ∼12−16% defluorination was achieved after 2 h of reaction according to the F^- measurements (Figures S12a and 3). To the best of our knowledge, this is the highest reductive defluorination rate of fluorinated organics by NZVI-based technologies at room temperature and pressure. Moreover, further defluorination after 15 days was expected according to the increasing trend of F^- ions and the added SNZVI would provide enough electrons (∼5−15 mM) for the reductive dechlorination and defluorination of 0.28 mM FF (2 mol e^- per mol Cl or F), especially since the water reactivity was greatly suppressed.

Notably, the defluorination became slower after 2 h and maintained that rate for over 1 day (Figure 3a). The generation of F^- fitted the zero-order kinetics, suggesting that the defluorination rate was controlled by the amount of reactive sites rather than the FF concentration.[66] The defluorination rates of FF (k_{SA,F^-}) by SNZVI in the first 2 h (in the presence of FF) were ∼130−220 times higher than those after 1 day (with only dideschloro FF (FF − 2Cl + 2H) present, i.e., after the dechlorination was complete) (Figure 3b), indicating the role of Cl in the defluorination reaction. DFT calculations were performed to study the adsorption affinities of FF and dechlorinated products onto the NZVI and SNZVI surfaces. Typical S positions close to and far away from the sulfonyl group in FF were included as representative configurations. DFT calculations show that the adsorption of the dechlorinated radical (deCl* intermediate) on either Fe(110) or S-on-Fe(110) surfaces is close to or even significantly stronger (i.e., more negative) than FF and dideschloro FF (Figures 3c and S13), suggesting that the dechlorination step would favor the adsorption and subsequent defluorination of the contaminant. In addition, the highly chemically reactive FF-adsorbed S-on-Fe(110) surface (Figure 2f,g) and the much stronger

https://dx.doi.org/10.1021/acs.est.0c07319
Environ. Sci. Technol. 2021, 55, 2628−2638

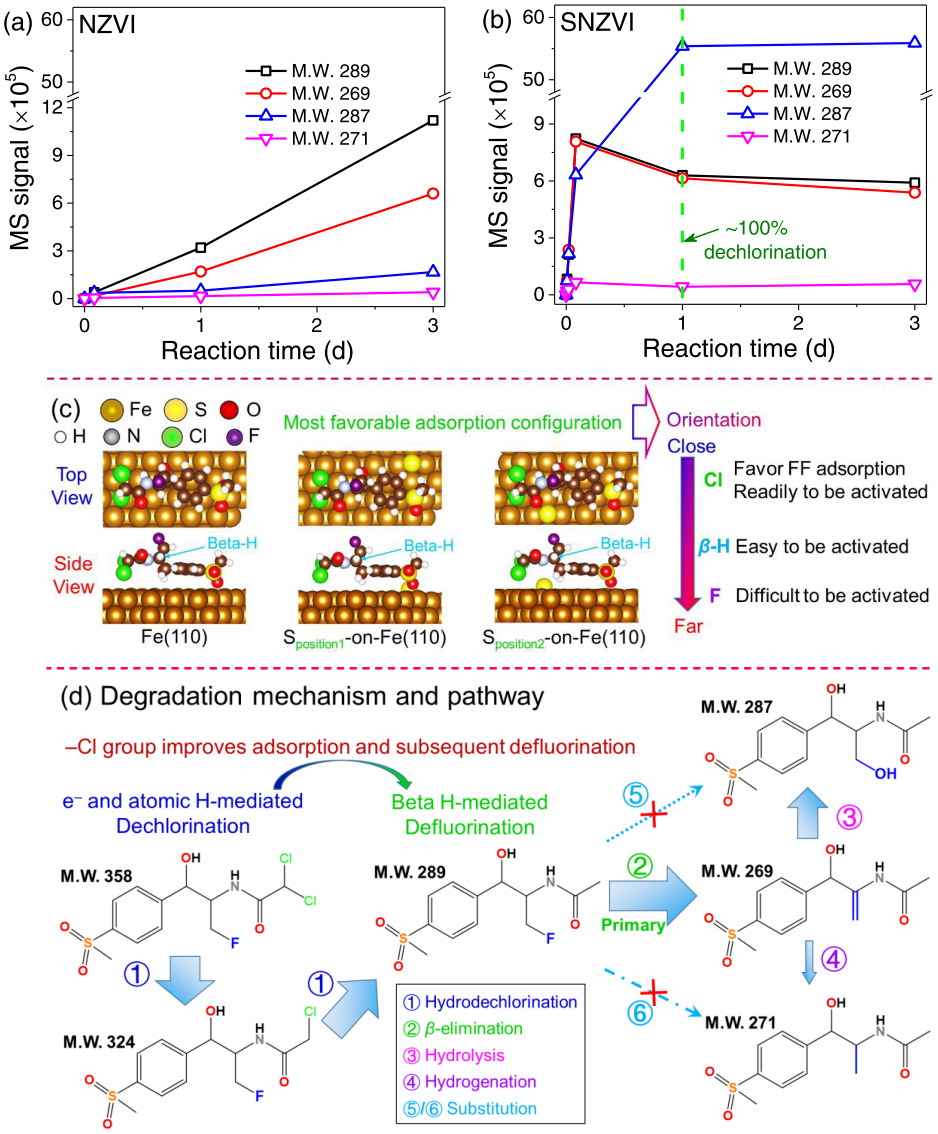

Figure 4. MS signals of dideschloro FF (MW 289) and three defluorinated products (MWs 269, 287, and 271) by (a) NZVI and (b) SNZVI with 0.13 $[S/Fe]_{particles}$ according to the UPLC-MS/MS analysis; the solid line is interpolated (not fit) and only meant to guide the eye. (c) Favorable adsorption configurations of FF on the Fe(110) and S-on-Fe(110) surfaces. (d) Degradation mechanism and pathway of FF by SNZVI.

adsorption of FF and/or the deCl* intermediate than dideschloro FF (Figure 3c) are also consistent with the faster defluorination in the presence of Cl groups (Figure 3b). There is a strong possibility that some molecules were successively dechlorinated and defluorinated before they left the S-on-Fe(110) surfaces, which is consistent with the product distribution as discussed later.

These benefits derived from the Cl-induced adsorption and dechlorination were the most likely reasons for the faster defluorination by SNZVI before complete dechlorination. Moreover, the defluorination by SNZVI was improved by 35 ± 9% after adding TBA (Figure 3d), which is a scavenger of both atomic H and hydroxyl radicals ($^{\bullet}OH$).[38,60] These results suggest that the Cl groups and slowed dechlorination (Figure 3b) could favor the defluorination, and atomic H and $^{\bullet}OH$ are unlikely to be the reactive species for defluorination via direct substitution.

3.5. Defluorination Mechanism by SNZVI. UPLC-MS/MS analysis was performed to gain an understanding of the degradation pathway of FF by SNZVI. Two dechlorinated products (molecular weights (MWs) 324 and 289) and three defluorinated products (MWs 269, 287, and 271) were detected according to the relative mass (Figures 4a,b and S14). Detailed chromatograms of UPLC-MS/MS are shown in Figures S14−S22. Note that the product MW 324 was transient due to rapid dechlorination. No directly defluorinated products of FF (either FF eliminated one F atom or FF eliminated one Cl atom and one F atom) were detected, further confirming that the Cl atom was removed prior to, or simultaneously with, the F atom. The defluorination of dideschloro FF (FF − 2Cl + 2H) could occur along with the dechlorination of deschloro FF (FF − Cl + H) because F^- (Figure 3a) and defluorinated products (e.g., MW 269) (Figure 4b) were detected before the complete dechlorination. This further indicates that the dechlorination and defluorination might occur "simultaneously" once the FF molecule is adsorbed on the surface, consistent with the fact that enhanced adsorption of the deCl* intermediate and FF could improve the defluorination.

https://dx.doi.org/10.1021/acs.est.0c07319
Environ. Sci. Technol. 2021, 55, 2628−2638

DFT calculations were used to theoretically elucidate the defluorination mechanism of FF by SNZVI. The most favorable adsorption configuration of FF on SNZVI surfaces (Figure 4c) indicates that: (i) sulfur does not affect the favorable adsorption configuration of FF on the surface, indicating the similar FF degradation pathway by NZVI and SNZVI, (ii) Cl is close to the surface but not chemically bound, and ready to be activated and will favorably dechlorinate first, (iii) C−F is kinetically difficult to activate as a subsequent step since the orientation of F is far away from the Fe surface, and (iv) the β-H of the carbon (β carbon) connected to the C−F group is easier to activate as it points toward the Fe surface. It was reported that C−F bond energy decreased after an external electron was transferred to fluorinated contaminants; this might make the defluorination easier.[67,68] Note that transition-metal (e.g., Mn, Fe, Co, and Ni)-catalyzed defluorination through β-elimination is well established in synthetic organic chemistry.[4,69,70] Reductive defluorination via β-elimination on metallic surfaces (e.g., Fe surface)[71] also indicates the potential of high-surface-area nanoscale iron particles for defluorination. In addition, β-elimination was also proposed to be the primary pathway of trichloroethylene (TCE) dechlorination by SNZVI according to the primary product C_2H_2 in previous studies.[12,13] This favorable adsorption configuration confirms that the C−Cl activation is a favorable step and β-elimination (where the H at the β carbon decomposes before the decomposition of F at the α carbon) can easily happen as compared to the direct activation of C−F (i.e., substitution by either atomic H or $^{\bullet}$OH radicals). This also supports a mechanism where dechlorination occurs before defluorination, and the Cl group would favor the adsorption and subsequent defluorination as previously discussed. The defluorination primarily via β-elimination is also consistent with the finding that the defluorination was inhibited at a high sulfur amount despite improved adsorption (Figure S23) because sulfur can block H adsorption at Fe sites and is expected to make the area nearby S inert to the activation of β-H (Figure 2d). This is also consistent with the observation that defluorination was inhibited after more α-H was generated during dechlorination, which is more active than the β-H. Note that the spin-polarized DFT calculations on these large adsorption configurations involve high computational cost. Due to the current qualitative agreement with experiments, we did not further evaluate the reaction kinetics in this study.

Based on the experimental data, DFT calculations, and UPLC-MS/MS analysis, the degradation mechanism of FF by SNZVI is explained (Figure 4c). Although H_2 evolution could be used as an indicator that positively correlates with both dechlorination and defluorination rates, H_2 is not the key species that can directly or indirectly be utilized to degrade FF. Rather, this is because the dechlorination and defluorination can occur via e^-/atomic H- and β-H-mediated reactions, respectively, and the higher generation of e^-/atomic H or favored activation of β-H leads to a faster H_2 evolution.

4. ENVIRONMENTAL IMPLICATIONS

Herein, we provide insight into the reactive sites and species of SNZVI for rapid dechlorination and relatively fast defluorination from bulk to atomistic perspectives and confirm the roles of Cl groups and dechlorination in defluorination. These will further advance the understanding of SNZVI nanoparticles for environmental remediation and help to rationally design SNZVI with properties and reactive sites/species tailored for specific application scenarios. For example, the hydrophobicity and the proportion of reactive species could potentially be tuned by controlling the S amount and speciation, providing different reactivity and selectivity toward hydrophobic organic contaminants (e.g., trichloroethylene) or hydrophilic inorganic contaminants (e.g., nitrate, heavy-metal ions).

The increased hydrophobicity and higher surface of the SNZVI obtained with the post-sulfidation method used here provide higher reactivity with hydrophobic contaminants and still suppress reactivity with water. The limited release of S (<0.08% of the actual S content), suppressed water reactivity, extended the reactive lifetime of SNZVI (∼840 days), and enhanced reactivity and selectivity for dechlorination and defluorination, indicating that this modified post-sulfidized SNZVI is a promising material for the in situ groundwater remediation of chlorinated and fluorinated organic contaminants. Since no FF was detected by the UPLC-MS/MS (limits of detection (LOD) = 0.01 ng L^{-1}) after the reaction with SNZVI, and the defluorination reaction with SNZVI occurs in natural matrices,[17] the defluorination reaction reported here should persist in a natural environment with low FF concentrations. In addition, higher defluorination rates are expected at high Fe/FF ratios.

Tuning the physicochemical properties (e.g., sulfur amount, morphology, and hydrophobicity) of SNZVI and applying it for fluorinated contaminants with Cl groups are expected to further improve its performance for defluorination. It can also guide the design of fluorinated substances considering both application and end disposal. The findings in this study can help to predict and elucidate the reactivity and mechanism of SNZVI for dehalogenation, to expand the application scenarios of SNZVI (e.g., for defluorination), and to inspire future efforts for continuously exploring other applications of SNZVI.

■ ASSOCIATED CONTENT

Supporting Information

The Supporting Information is available free of charge at https://pubs.acs.org/doi/10.1021/acs.est.0c07319.

Additional information of dechlorination rate of FF removal by SNZVI with an Fe^{2+} or Fe^{3+} precursor; TEM images of NZVI and conventional post-sulfidized SNZVI; TEM images and element distributions of SNZVI; hydrophobicity; Fe^0 content; surface area; electrochemical tests and hydrogen evolution of NZVI and SNZVI; FF and its product distribution with or without TBA; and UPLC-MS/MS spectra (PDF)

■ AUTHOR INFORMATION

Corresponding Author

Jiang Xu − *College of Environmental and Resource Sciences, Zhejiang University, Hangzhou 310058, China; Department of Civil and Environmental Engineering, Carnegie Mellon University, Pittsburgh, Pennsylvania 15213, United States;* orcid.org/0000-0003-0369-4848; Email: xujiang6@zju.edu.cn

Authors

Zhen Cao − *College of Environmental and Resource Sciences, Zhejiang University, Hangzhou 310058, China*

Hao Li − *Department of Chemistry and Oden Institute for Computational Engineering and Sciences, The University of*

https://dx.doi.org/10.1021/acs.est.0c07319
Environ. Sci. Technol. 2021, 55, 2628−2638

Texas at Austin, Austin, Texas 78712, United States; orcid.org/0000-0002-7577-1366

Gregory V. Lowry − *Department of Civil and Environmental Engineering, Carnegie Mellon University, Pittsburgh, Pennsylvania 15213, United States;* orcid.org/0000-0001-8599-008X

Xiaoyang Shi − *Earth Engineering Center, Center for Advanced Materials for Energy and Environment, Department of Earth and Environmental Engineering, Columbia University, New York 10027, United States*

Xiangcheng Pan − *State Key Laboratory of Molecular Engineering of Polymers, Department of Macromolecular Science, Fudan University, Shanghai 200438, China;* orcid.org/0000-0003-3344-4639

Xinhua Xu − *College of Environmental and Resource Sciences, Zhejiang University, Hangzhou 310058, China*

Graeme Henkelman − *Department of Chemistry and Oden Institute for Computational Engineering and Sciences, The University of Texas at Austin, Austin, Texas 78712, United States;* orcid.org/0000-0002-0336-7153

Complete contact information is available at: https://pubs.acs.org/10.1021/acs.est.0c07319

Notes

The authors declare no competing financial interest.

■ ACKNOWLEDGMENTS

This work was supported by the National Science Foundation (NSF) and the Environmental Protection Agency (EPA) under NSF Cooperative Agreement EF-0830093 and DBI-1266252 to G.V.L., and the National Natural Science Foundation of China (no. 21976153). The calculations were supported by the Welch Foundation (F-1841) and the Texas Advanced Computing Center.

■ REFERENCES

(1) Ahrens, T.; Kohlmann, J.; Ahrens, M.; Braun, T. Functionalization of Fluorinated Molecules by Transition-Metal-Mediated C−F Bond Activation to Access Fluorinated Building Blocks. *Chem. Rev.* **2015**, *115*, 931−972.

(2) Colomban, C.; Kudrik, E. V.; Afanasiev, P.; Sorokin, A. B. Catalytic Defluorination of Perfluorinated Aromatics Under Oxidative Conditions Using N-Bridged Diiron Phthalocyanine. *J. Am. Chem. Soc.* **2014**, *136*, 11321−11330.

(3) Cui, B.; Jia, S.; Tokunaga, E.; Shibata, N. Defluorosilylation of Fluoroarenes and Fluoroalkanes. *Nat. Commun.* **2018**, *9*, No. 4393.

(4) Huang, Y.; Hayashi, T. Rhodium-Catalyzed Asymmetric Arylation/Defluorination of 1-(Trifluoromethyl)Alkenes Forming Enantioenriched 1,1-Difluoroalkenes. *J. Am. Chem. Soc.* **2016**, *138*, 12340−12343.

(5) Liu, Y.; Majetich, S. A.; Tilton, R. D.; Sholl, D. S.; Lowry, G. V. TCE Dechlorination Rates, Pathways, and Efficiency of Nanoscale Iron Particles with Different Properties. *Environ. Sci. Technol.* **2005**, *39*, 1338−1345.

(6) Fu, F.; Dionysiou, D. D.; Liu, H. The Use of Zero-Valent Iron for Groundwater Remediation and Wastewater Treatment: A Review. *J. Hazard. Mater.* **2014**, *267*, 194−205.

(7) He, F.; Zhao, D. Preparation and Characterization of a New Class of Starch-Stabilized Bimetallic Nanoparticles for Degradation of Chlorinated Hydrocarbons in Water. *Environ. Sci. Technol.* **2005**, *39*, 3314−3320.

(8) Ling, L.; Zhang, W. Enrichment and Encapsulation of Uranium with Iron Nanoparticle. *J. Am. Chem. Soc.* **2015**, *137*, 2788−2791.

(9) Park, S.; Zenobio, J. E.; Lee, L. S. Perfluorooctane Sulfonate (PFOS) Removal with Pd^0/nFe^0 Nanoparticles: Adsorption Or Aqueous Fe-Complexation, Not Transformation? *J. Hazard. Mater.* **2018**, *342*, 20−28.

(10) Blotevogel, J.; Giraud, R. J.; Borch, T. Reductive Defluorination of Perfluorooctanoic Acid by Zero-Valent Iron and Zinc: A DFT-Based Kinetic Model. *Chem. Eng. J.* **2018**, *335*, 248−254.

(11) Qin, H.; Guan, X.; Bandstra, J. Z.; Johnson, R. L.; Tratnyek, P. G. Modeling the Kinetics of Hydrogen Formation by Zerovalent Iron: Effects of Sulfidation On Micro- And Nano-Scale Particles. *Environ. Sci. Technol.* **2018**, *52*, 13887−13896.

(12) He, F.; Li, Z.; Shi, S.; Xu, W.; Sheng, H.; Gu, Y.; Jiang, Y.; Xi, B. Dechlorination of Excess Trichloroethene by Bimetallic and Sulfidated Nanoscale Zero-Valent Iron. *Environ. Sci. Technol.* **2018**, *52*, 8627−8637.

(13) Xu, J.; Wang, Y.; Weng, C.; Bai, W.; Jiao, Y.; Kaegi, R.; Lowry, G. V. Reactivity, Selectivity, and Long-Term Performance of Sulfidized Nanoscale Zerovalent Iron with Different Properties. *Environ. Sci. Technol.* **2019**, *53*, 5936−5945.

(14) Su, Y.; Lowry, G. V.; Jassby, D.; Zhang, Y. Sulfide-Modified NZVI (S-NZVI): Synthesis, Characterization, and Reactivity. *Nanoscale Zerovalent Iron Particles for Environmental Restoration*; Springer: Cham, 2019; pp 359−386.

(15) Fan, D.; Lan, Y.; Tratnyek, P. G.; Johnson, R. L.; Filip, J.; O Carroll, D. M.; Nunez Garcia, A.; Agrawal, A. Sulfidation of Iron-Based Materials: A Review of Processes and Implications for Water Treatment and Remediation. *Environ. Sci. Technol.* **2017**, *51*, 13070−13085.

(16) Song, S.; Su, Y.; Adeleye, A. S.; Zhang, Y.; Zhou, X. Optimal Design and Characterization of Sulfide-Modified Nanoscale Zerovalent Iron for Diclofenac Removal. *Appl. Catal., B* **2017**, *201*, 211−220.

(17) Cao, Z.; Liu, X.; Xu, J.; Zhang, J.; Yang, Y.; Zhou, J.; Xu, X.; Lowry, G. V. Removal of Antibiotic Florfenicol by Sulfide-Modified Nanoscale Zero-Valent Iron. *Environ. Sci. Technol.* **2017**, *51*, 11269−11277.

(18) Mangayayam, M.; Dideriksen, K.; Ceccato, M.; Tobler, D. J. The Structure of Sulfidized Zero-Valent Iron by One-Pot Synthesis: Impact On Contaminant Selectivity and Long-Term Performance. *Environ. Sci. Technol.* **2019**, *53*, 4389−4396.

(19) Li, J.; Zhang, X.; Sun, Y.; Liang, L.; Pan, B.; Zhang, W.; Guan, X. Advances in Sulfidation of Zerovalent Iron for Water Decontamination. *Environ. Sci. Technol.* **2017**, *51*, 13533−13544.

(20) Xu, J.; Avellan, A.; Li, H.; Liu, X.; Noël, V.; Lou, Z.; Wang, Y.; Kaegi, R.; Henkelman, G.; Lowry, G. V. Sulfur Loading and Speciation Control the Hydrophobicity, Electron Transfer, Reactivity, and Selectivity of Sulfidized Nanoscale Zerovalent Iron. *Adv. Mater.* **2020**, *32*, No. 1906910.

(21) Wang, X.; Xu, C.; Jaroniec, M.; Zheng, Y.; Qiao, S. Anomalous Hydrogen Evolution Behavior in High-pH Environment Induced by Locally Generated Hydronium Ions. *Nat. Commun.* **2019**, *10*, No. 4876.

(22) Jiang, G.; Lan, M.; Zhang, Z.; Lv, X.; Lou, Z.; Xu, X.; Dong, F.; Zhang, S. Identification of Active Hydrogen Species On Palladium Nanoparticles for an Enhanced Electrocatalytic Hydrodechlorination of 2,4-Dichlorophenol in Water. *Environ. Sci. Technol.* **2017**, *51*, 7599−7605.

(23) Wang, J.; Farrell, J. Investigating the Role of Atomic Hydrogen On Chloroethene Reactions with Iron Using Tafel Analysis and Electrochemical Impedance Spectroscopy. *Environ. Sci. Technol.* **2003**, *37*, 3891−3896.

(24) Kim, E. J.; Kim, J. H.; Azad, A. M.; Chang, Y. S. Facile Synthesis and Characterization of Fe/FeS Nanoparticles for Environmental Applications. *ACS Appl. Mater. Interfaces* **2011**, *3*, 1457−1462.

(25) Su, Y.; Adeleye, A. S.; Keller, A. A.; Huang, Y.; Dai, C.; Zhou, X.; Zhang, Y. Magnetic Sulfide-Modified Nanoscale Zerovalent Iron (S-NZVI) for Dissolved Metal Ion Removal. *Water Res.* **2015**, *74*, 47−57.

(26) Tang, J.; Tang, L.; Feng, H.; Zeng, G.; Dong, H.; Zhang, C.; Huang, B.; Deng, Y.; Wang, J.; Zhou, Y. pH-Dependent Degradation of p-Nitrophenol by Sulfidated Nanoscale Zerovalent Iron Under

Aerobic Or Anoxic Conditions. *J. Hazard. Mater.* **2016**, *320*, 581−590.
(27) Xu, J.; Avellan, A.; Li, H.; Clark, E. A.; Henkelman, G.; Kaegi, R.; Lowry, G. V. Iron and Sulfur Precursors Affect Crystalline Structure, Speciation, and Reactivity of Sulfidized Nanoscale Zerovalent Iron. *Environ. Sci. Technol.* **2020**, *54*, 13294−13303.
(28) Cao, Z.; Xu, J.; Li, H.; Ma, T.; Lou, L.; Henkelman, G.; Xu, X. Dechlorination and Defluorination Capability of Sulfidized Nanoscale Zerovalent Iron with Suppressed Water Reactivity. *Chem. Eng. J.* **2020**, *400*, No. 125900.
(29) Zhang, Q.; Ying, G.; Pan, C.; Liu, Y.; Zhao, J. Comprehensive Evaluation of Antibiotics Emission and Fate in the River Basins of China: Source Analysis, Multimedia Modeling, and Linkage to Bacterial Resistance. *Environ. Sci. Technol.* **2015**, *49*, 6772−6782.
(30) Zhao, H.; Cao, Z.; Liu, X.; Zhan, Y.; Zhang, J.; Xiao, X.; Yang, Y.; Zhou, J.; Xu, J. Seasonal Variation, Flux Estimation, and Source Analysis of Dissolved Emerging Organic Contaminants in the Yangtze Estuary, China. *Mar. Pollut. Bull.* **2017**, *125*, 208−215.
(31) Wang, C.; Zhang, W. Synthesizing Nanoscale Iron Particles for Rapid and Complete Dechlorination of TCE and PCBs. *Environ. Sci. Technol.* **1997**, *31*, 2154−2156.
(32) Rajajayavel, S. R.; Ghoshal, S. Enhanced Reductive Dechlorination of Trichloroethylene by Sulfidated Nanoscale Zerovalent Iron. *Water Res.* **2015**, *78*, 144−153.
(33) Xu, C.; Zhang, B.; Wang, Y.; Shao, Q.; Zhou, W.; Fan, D.; Bandstra, J. Z.; Shi, Z.; Tratnyek, P. G. Effects of Sulfidation, Magnetization, and Oxygenation On Azo Dye Reduction by Zerovalent Iron. *Environ. Sci. Technol.* **2016**, *50*, 11879−11887.
(34) Shao, Q.; Xu, C.; Wang, Y.; Huang, S.; Zhang, B.; Huang, L.; Fan, D.; Tratnyek, P. G. Dynamic Interactions Between Sulfidated Zerovalent Iron and Dissolved Oxygen: Mechanistic Insights for Enhanced Chromate Removal. *Water Res.* **2018**, *135*, 322−330.
(35) Lymar, S. V.; Schwarz, H. A. Hydrogen Atom Reactivity Toward Aqueous Tert-Butyl Alcohol. *J. Phys. Chem. A* **2012**, *116*, 1383−1389.
(36) Wojnárovits, L.; Takács, E.; Dajka, K.; Emmi, S. S.; Russo, M.; D Angelantonio, M. Re-Evaluation of the Rate Constant for the H Atom Reaction with Tert-Butanol in Aqueous Solution. *Radiat. Phys. Chem.* **2004**, *69*, 217−219.
(37) Lou, Z.; Zhou, J.; Sun, M.; Xu, J.; Yang, K.; Lv, D.; Zhao, Y.; Xu, X. MnO_2 Enhances Electrocatalytic Hydrodechlorination by Pd/Ni Foam Electrodes and Reduces Pd Needs. *Chem. Eng. J.* **2018**, *352*, 549−557.
(38) Anipsitakis, G. P.; Dionysiou, D. D. Radical Generation by the Interaction of Transition Metals with Common Oxidants. *Environ. Sci. Technol.* **2004**, *38*, 3705−3712.
(39) Zhang, Y.; Jiang, H.; Zhang, Y.; Xie, J. The Dispersity-Dependent Interaction Between Montmorillonite Supported NZVI and Cr(VI) in Aqueous Solution. *Chem. Eng. J.* **2013**, *229*, 412−419.
(40) Bhattacharjee, S.; Ghoshal, S. Optimal Design of Sulfidated Nanoscale Zerovalent Iron for Enhanced Trichloroethene Degradation. *Environ. Sci. Technol.* **2018**, *52*, 11078−11086.
(41) Xu, J.; Cao, Z.; Zhou, H.; Lou, Z.; Wang, Y.; Xu, X.; Lowry, G. V. Sulfur Dose and Sulfidation Time Affect Reactivity and Selectivity of Post-Sulfidized Nanoscale Zerovalent Iron. *Environ. Sci. Technol.* **2019**, *53*, 13344−13352.
(42) Cao, Z.; Li, H.; Xu, X.; Xu, J. Correlating Surface Chemistry and Hydrophobicity of Sulfidized Nanoscale Zerovalent Iron with its Reactivity and Selectivity for Denitration and Dechlorination. *Chem. Eng. J.* **2020**, *394*, No. 124876.
(43) Xu, J.; Cao, Z.; Wang, Y.; Zhang, Y.; Gao, X.; Ahmed, M. B.; Zhang, J.; Yang, Y.; Zhou, J. L.; Lowry, G. V. Distributing Sulfidized Nanoscale Zerovalent Iron Onto Phosphorus-Functionalized Biochar for Enhanced Removal of Antibiotic Florfenicol. *Chem. Eng. J.* **2019**, *359*, 713−722.
(44) Xu, H.; Sun, Y.; Li, J.; Li, F.; Guan, X. Aging of Zerovalent Iron in Synthetic Groundwater: X-Ray Photoelectron Spectroscopy Depth Profiling Characterization and Depassivation with Uniform Magnetic Field. *Environ. Sci. Technol.* **2016**, *50*, 8214−8222.
(45) Lv, D.; Zhou, J.; Cao, Z.; Xu, J.; Liu, Y.; Li, Y.; Yang, K.; Lou, Z.; Lou, L.; Xu, X. Mechanism and Influence Factors of Chromium(VI) Removal by Sulfide-Modified Nanoscale Zerovalent Iron. *Chemosphere* **2019**, *224*, 306−315.
(46) Li, J.; Zhang, X.; Liu, M.; Pan, B.; Zhang, W.; Shi, Z.; Guan, X. Enhanced Reactivity and Electron Selectivity of Sulfidated Zerovalent Iron Toward Chromate Under Aerobic Conditions. *Environ. Sci. Technol.* **2018**, *52*, 2988−2997.
(47) Su, Y.; Jassby, D.; Zhang, Y.; Keller, A. A.; Adeleye, A. S. Comparison of the Colloidal Stability, Mobility, and Performance of Nanoscale Zerovalent Iron and Sulfidated Derivatives. *J. Hazard. Mater.* **2020**, *396*, No. 122691.
(48) Xu, J.; Cao, Z.; Liu, X.; Zhao, H.; Xiao, X.; Wu, J.; Xu, X.; Zhou, J. L. Preparation of Functionalized Pd/Fe-Fe_3O_4@MWCNTs Nanomaterials for Aqueous 2,4-Dichlorophenol Removal: Interactions, Influence Factors, and Kinetics. *J. Hazard. Mater.* **2016**, *317*, 656−666.
(49) Xu, J.; Liu, X.; Lowry, G. V.; Cao, Z.; Zhao, H.; Zhou, J. L.; Xu, X. Dechlorination Mechanism of 2,4-Dichlorophenol by Magnetic MWCNTs Supported Pd/Fe Nanohybrids: Rapid Adsorption, Gradual Dechlorination, and Desorption of Phenol. *ACS Appl. Mater. Interfaces* **2016**, *8*, 7333−7342.
(50) Blöchl, P. E. Projector Augmented-Wave Method. *Phys. Rev. B* **1994**, *50*, 17953−17979.
(51) Perdew, J. P.; Burke, K.; Ernzerhof, M. Generalized Gradient Approximation Made Simple. *Phys. Rev. Lett.* **1996**, *77*, 3865−3868.
(52) Kohn, W.; Sham, L. J. Self-Consistent Equations Including Exchange and Correlation Effects. *Phys. Rev.* **1965**, *140*, A1133−A1138.
(53) Monkhorst, H. J.; Pack, J. D. Special Points for Brillouin-Zone Integrations. *Phys. Rev. B* **1976**, *13*, 5188−5192.
(54) Phenrat, T.; Saleh, N.; Sirk, K.; Tilton, R. D.; Lowry, G. V. Aggregation and Sedimentation of Aqueous Nanoscale Zerovalent Iron Dispersions. *Environ. Sci. Technol.* **2007**, *41*, 284−290.
(55) Kocabag, D.; Shergold, H. L.; Kelsall, G. H. Natural Oleophilicity/Hydrophobicity of Sulphide Minerals, II. Pyrite. *Int. J. Miner. Process.* **1990**, *29*, 211−219.
(56) Hicyilmaz, C.; Emre Altun, N.; Ekmekci, Z.; Gokagac, G. Quantifying Hydrophobicity of Pyrite After Copper Activation and DTPI Addition Under Electrochemically Controlled Conditions. *Miner. Eng.* **2004**, *17*, 879−890.
(57) Liu, X.; Cao, Z.; Yuan, Z.; Zhang, J.; Guo, X.; Yang, Y.; He, F.; Zhao, Y.; Xu, J. Insight Into the Kinetics and Mechanism of Removal of Aqueous Chlorinated Nitroaromatic Antibiotic Chloramphenicol by Nanoscale Zero-Valent Iron. *Chem. Eng. J.* **2018**, *334*, 508−518.
(58) Liu, Y.; Wu, T.; White, J. C.; Lin, D. A New Strategy Using Nanoscale Zero-Valent Iron to Simultaneously Promote Remediation and Safe Crop Production in Contaminated Soil. *Nat. Nanotechnol.* **2020**, DOI: 10.1038/s41565-020-00803-1.
(59) Wu, D.; Peng, S.; Yan, K.; Shao, B.; Feng, Y.; Zhang, Y. Enhanced As(III) Sequestration Using Sulfide-Modified Nano-Scale Zero-Valent Iron with a Characteristic Core−Shell Structure: Sulfidation and As Distribution. *ACS Sustainable Chem. Eng.* **2018**, *6*, 3039−3048.
(60) Liu, H.; Han, J.; Yuan, J.; Liu, C.; Wang, D.; Liu, T.; Liu, M.; Luo, J.; Wang, A.; Crittenden, J. C. Deep Dehalogenation of Florfenicol Using Crystalline CoP Nanosheet Arrays On a Ti Plate Via Direct Cathodic Reduction and Atomic H. *Environ. Sci. Technol.* **2019**, *53*, 11932−11940.
(61) Han, Y.; Yan, W. Reductive Dechlorination of Trichloroethene by Zero-Valent Iron Nanoparticles: Reactivity Enhancement through Sulfidation Treatment. *Environ. Sci. Technol.* **2016**, *50*, 12992−13001.
(62) Wei, L.; Li, H.; Chen, J.; Yuan, Z.; Huang, Q.; Liao, X.; Henkelman, G.; Chen, Y. Thiocyanate-Modified Silver Nanofoam for Efficient CO_2 Reduction to CO. *ACS Catal.* **2020**, *10*, 1444−1453.
(63) Yu, H.; Li, J.; Zhang, Y.; Yang, S.; Han, K.; Dong, F.; Ma, T.; Huang, H. Three-in-One Oxygen Vacancies: Whole Visible-Spectrum Absorption, Efficient Charge Separation, and Surface Site Activation

for Robust CO_2 Photoreduction. *Angew. Chem., Int. Ed.* **2019**, *58*, 3880−3884.
(64) Hammer, B.; Norskov, J. K. Why Gold is the Noblest of All the Metals. *Nature* **1995**, *376*, 238−240.
(65) Liang, Z.; Ahn, H. S.; Bard, A. J. A Study of the Mechanism of the Hydrogen Evolution Reaction On Nickel by Surface Interrogation Scanning Electrochemical Microscopy. *J. Am. Chem. Soc.* **2017**, *139*, 4854−4858.
(66) Wüst, W. F.; Köber, R.; Schlicker, O.; Dahmke, A. Combined Zero- And First-Order Kinetic Model of the Degradation of TCE and cis-DCE with Commercial Iron. *Environ. Sci. Technol.* **1999**, *33*, 4304−4309.
(67) Rao, U.; Su, Y.; Khor, C. M.; Jung, B.; Ma, S.; Cwiertny, D. M.; Wong, B. M.; Jassby, D. Structural Dependence of Reductive Defluorination of Linear PFAS Compounds in a UV/Electrochemical System. *Environ. Sci. Technol.* **2020**, *54*, 10668−10677.
(68) Su, Y.; Rao, U.; Khor, C. M.; Jensen, M. G.; Teesch, L. M.; Wong, B. M.; Cwiertny, D. M.; Jassby, D. Potential-Driven Electron Transfer Lowers the Dissociation Energy of the C−F Bond and Facilitates Reductive Defluorination of Perfluorooctane Sulfonate (PFOS). *ACS Appl. Mater. Interfaces* **2019**, *11*, 33913−33922.
(69) Fujita, T.; Fuchibe, K.; Ichikawa, J. Transition-Metal-Mediated and -Catalyzed C−F Bond Activation by Fluorine Elimination. *Angew. Chem., Int. Ed.* **2019**, *58*, 390−402.
(70) Ichitsuka, T.; Fujita, T.; Arita, T.; Ichikawa, J. Double C−F Bond Activation through β-Fluorine Elimination: Nickel-Mediated [3+2] Cycloaddition of 2-Trifluoromethyl-1-Alkenes with Alkynes. *Angew. Chem., Int. Ed.* **2014**, *53*, 7564−7568.
(71) Kiplinger, J. L.; Richmond, T. G.; Osterberg, C. E. Activation of Carbon-Fluorine Bonds by Metal Complexes. *Chem. Rev.* **1994**, *94*, 373−431.

https://dx.doi.org/10.1021/acs.est.0c07319
Environ. Sci. Technol. 2021, 55, 2628−2638